Accelerated Publications

Combined Microspectrophotometric and Crystallographic Examination of Chemically Reduced and X-ray Radiation-Reduced Forms of Cytochrome ba_3 Oxidase from *Thermus thermophilus*: Structure of the Reduced Form of the Enzyme[†]

Bin Liu,[‡] Ying Chen,[‡] Tzanko Doukov,[§] S. Michael Soltis,*[,§] C. David Stout,*[,‡] and James A. Fee*[,‡]

Department of Molecular Biology, The Scripps Research Institute, MB-8, 10550 North Torrey Pines Road, La Jolla, California 92037, and Stanford Synchrotron Radiation Laboratory, 2575 Sand Hill Road, Menlo Park, California 94025

Received September 15, 2008; Revised Manuscript Received December 22, 2008

ABSTRACT: Three paths for obtaining crystals of reduced (II-E4Q/I-K258R) cytochrome ba_3 are described, and the structures of these are reported at ~2.8−3.0 Å resolution. Microspectrophotometry of single crystals of *Thermus* ba_3 oxidase at 100 K was used to show that crystals of the oxidized enzyme are reduced in an intense X-ray (beam line 7-1 at the Stanford Synchrotron Radiation Laboratory), being nearly complete in 1 min. The previously reported structures of ba_3 (Protein Data Bank entries
and
), having a crystallographically detectable water between the Cu_B and Fe_{a3} metals of the dinuclear center, actually represent the X-ray radiation-reduced enzyme. Dithionite-reduced crystals or crystals formed from dithionite-reduced enzyme revealed the absence of the above-mentioned water and an increase in the Cu_B-Fe_{a3} distance of ~0.3 A. The new structures are discussed in terms of enzyme function. An unexpected optical absorption envelope at ~590 nm is also reported. This spectral feature is tentatively thought to arise from a five-coordinate, low-spin, ferrous heme a_3 that is trapped in the frozen crystals.

In respiring organisms, cytochrome *c* oxidase catalyzes proton translocation coupled to the reduction of O_2 to water (*1, 2*). Cytochrome ba_3 oxidase is one of two heme-copper oxidases isolated from *Thermus thermophilus* (*3*). It contains the dinuclear Cu_A center; a six-coordinate, low-spin (6cLS)[1] heme B; and a (usually) five-coordinate, high-spin (5cHS) heme A_s in the proximity of Cu_B (refs *3* and *4* and references cited therein). The latter (heme A_s and Cu_B) constitute the bimetallic site, and it is widely agreed that dioxygen binds to this site as the first step in O_2 reduction and proton pumping. Two crystal structures of native and recombinant, oxidized ba_3-type cytochrome *c* oxidase have been determined at <2.5 Å resolution (*5, 6*). However, the structure of reduced cytochrome ba_3 oxidase has not been reported.

Oxidized and reduced forms of cytochrome *c* oxidase represent two important intermediates in its catalytic cycle, and one might expect differences in their structures. In particular, the reduced enzyme should be structurally prepared to bind O_2 (*7, 8*). However, such structures obtained so far for the A1-type (*9*) enzymes indicate very small, if any, changes near the redox centers (*10*−*12*). Reported structures of both redox states from cytochrome aa_3 of *Paracoccus denitrificans* also revealed essentially no changes at 3.0−3.3 Å resolution (*10*), while in the case of bovine heart cytochrome *c* oxidase (also of the aa_3 type, and at a higher resolution), a redox-linked conformational change was observed in a surface loop (*13*) not present, for example, in cytochrome ba_3.

We recently reported the structure of a doubly mutated form of cytochrome ba_3 (II-E4Q/I-K258R) that forms robust

[†] Supported by NIH Grant GM35342 (J.A.F.). Part of this research was carried out at the Stanford Synchrotron Radiation Laboratory (SSRL), a national user facility operated by Stanford University on behalf of the U.S. Department of Energy, Office of Basic Energy Sciences. The SSRL Structural Molecular Biology Program is supported by the Department of Energy, Office of Biological and Environmental Research, and by the National Institutes of Health, National Center for Research Resources, Biomedical Technology Program, and the National Institute of General Medical Sciences.

* To whom correspondence should be addressed. C.D.S.: e-mail, dave@scripps.edu; telephone, (858) 784-8738; fax, (858) 784-2857. J.A.F.: e-mail, jafee@scripps.edu; telephone, (858) 784-9235; fax, (858) 784-2857. S.M.S.: e-mail, soltis@slac.stanford.edu; telephone, (650) 926-3050; fax, (650) 926-3292.

[‡] The Scripps Research Institute.

[§] Stanford Synchrotron Radiation Laboratory.

[1] Abbreviations: 5cLS, five-coordinate, low-spin; 5cHS, five-coordinate, high-spin; 6cLS, six-coordinate, low-spin.

10.1021/bi801759a CCC: $40.75
Published on Web 01/13/2009

crystals in just a few days due to a new lattice contact (*14*). This form of the enzyme is used throughout this work to examine properties and structures of the chemically reduced enzyme. By recording optical absorption spectra from single crystals before and after exposure to the X-ray beam, we gained new information about the redox state of the two hemes. Small but significant, and possibly important, structural changes were detected around the $Fe_{a3}-Cu_B$ dinuclear center. These changes, observed for defined spectroscopic states, support a direct, as opposed to an indirect (*15*), mechanism for the B-type oxidases (see ref *7*). The structures provide important new information about how the enzyme functions.

EXPERIMENTAL PROCEDURES

Protein Expression, Purification, and Crystallization. The mutant (II-E4Q/I-K258R) cytochrome ba_3 oxidase from *T. thermophilus* was expressed and purified as previously described (*14, 16*) and used throughout this study. Detergent exchange was conducted using DEAE resin (GE Science) in Econo-Column (Bio-Rad) (*14*). The purified protein sample was eluted and concentrated in 13 mM *n*-nonyl β-D-glucopyranoside (2 × CMC) in 10 mM Bis-Tris (pH 7.0) with 0.1 M KCl. The oxidized protein was crystallized under the same conditions as the recombinant wild type (*6*). Crystals ranged from ~250 to ~400 μm along their largest dimension. The concentration of enzyme within the unit cell is ~6 mM. To crystallize reduced mutant cytochrome ba_3, 5−10 mM sodium dithionite (Sigma, La Jolla, CA) was used. Moreover, all solutions used in the experiment were degassed, and the entire crystallization−archiving procedure was conducted in a glovebox at <1 ppm O_2 (COY Laboratory Products Inc.) filled with a gas mixture of 10% hydrogen and 90% nitrogen.

Single-Crystal Microspectrophotometry. Absorbance spectra of crystals mounted in an Oxford cryo-stream operating at ~100 K were recorded using either an in-house system based on an Ocean Optics USB4000 spectrometer or a modified 4DX system (*17*) installed at the Stanford Synchrotron Radiation Laboratory (SSRL) on beamline 7-1, which utilizes an Ocean Optics QE65000 spectrometer. All crystals were exposed to degassed cryoprotectant, typically 50% methylpentanediol, for ~10 s before being cryocooled and before the spectra were recorded. In the X-ray radiation-induced reduction experiments, crystal orientation was chosen to produce a satisfactory spectrum, and this was maintained in subsequent measurements. Spectral figures were prepared using IgorPro.

X-ray Data Collection. Where indicated, the cryoprotectant used previously (*14*) was supplemented with sodium dithionite (10 mM). This level of reductant was included to prevent oxidation of the enzyme during the time that the crystals were being transferred to liquid nitrogen. All data sets were collected on beamline 7-1 at SSRL at ~100 K, a wavelength of 0.979 Å, and an approximate total flux of 1×10^{13} photons/min.

Structure Determination and Refinement. All diffraction data were processed with MOSFLM and SCALA [CCP4 suite (*18*)]. The wild-type, recombinant structure (Protein Data Bank entry 1XME) was the initial model for molecular replacement with PHASER (*19*). The determined structures were then refined using rigid refinement and further restrained refinement with REFMAC 5.0 (*20*). For all data sets, 5% of the reflections were randomly selected to provide a test set for R_{free} calculations (*21*). Water molecules were placed in at least three σ positive peaks in the $F_o - F_c$ map and refined. Structure models and electron density maps were displayed with COOT (*22*).

Table 1: Data Collection and Refinement Statistics

	A path	B path	C path
beamline (SSRL)	7-1	7-1	7-1
resolution (Å)	3.10 (3.18−3.10)[a]	2.90 (2.98−2.90)[a]	2.80 (2.87−2.80)[a]
$P4_12_12$ cell dimensions (Å)			
$a = b$	119.75	120.85	115.63
c	150.81	150.40	149.17
solvent content (%)	54.9	55.5	51.0
total no. of observations	54047	96770	95862
no. of unique reflections	19624	25168	25479
redundancy	2.8 (2.3)[a]	3.8 (4.2)[a]	3.8 (4.0)[a]
completeness (%)	96.3 (96.3)[a]	99.4 (99.4)[a]	99.6 (99.6)[a]
$\langle I/\sigma_I \rangle$	5.9 (1.8)[a]	9.1 (1.8)[a]	7.1 (1.8)[a]
R_{sym}[b] (%)	7.4 (39.9)[a]	3.6 (35.4)[a]	4.4 (38.1)[a]
root-mean-square deviations			
bond lengths (Å)	0.024	0.022	0.020
bond angles (deg)	2.7	2.4	2.2
R_{work}/R_{free}[c] (%)	20.8/30.7	20.8/27.8	20.9/27.1
Protein Data Bank entry	3EH3	3EH4	3EH5

[a] Values in parentheses are for the last shell. [b] $R_{sym} = \sum I - \langle I \rangle / \sum I$, where I is the integrated intensity for a reflection. [c] R_{free} is the conventional crystallographic R factor, R_{work}, calculated on 5% of the data excluded from the refinement.

Coordinates of Fe_{a3} and Cu_B were refined against the anomalous difference data with MLPHARE (*18*) to independently determine the distance between them ($f' = 0.3$ e$^-$ and $f'' = 1.5$ e$^-$ for Fe; $f' = 0.0$ e$^-$ and $f'' = 2.2$ e$^-$ for Cu at 0.979 Å). The SCALA mtz files containing $|F^+|$ and $|F^-|$ to the resolution limit of each data set were used with a $6\sigma_{\Delta F}$ cutoff. The observed standard deviation of the coordinate shift of the $Fe_{a3}-Cu_B$ sites is very small for each data set, with the estimated error for the metal−metal distance being approximately ±0.03 Å. However, the metal−metal distances vary from data set to data set, i.e., different crystals, and for this reason, they are reported only to the first decimal place (see Table SI_1 of the Supporting Information). Refinement of Xe and Kr positions within ba_3 was carried out in a similar manner (see ref *8*).

VOIDOO (*23*) was utilized to compute the O_2 channel to include the cavity formed in the dinuclear site in the reduced structure (grid for plot files, 0.7 Å; probe radius, 1.0 Å). Figures were created using PyMOL (*24*). Details of data collection statistics and final refinement statistics are given in Table 1.

RESULTS

Crystals of reduced cytochrome ba_3 suitable for X-ray diffraction studies can be obtained (A path) by treatment of crystals of the oxidized, as-isolated protein with a cryoprotectant solution containing excess dithionite followed by a plunge into liquid nitrogen, (B path) by X-ray irradiation of crystals of oxidized protein maintained in a cryostream, and (C path) by growth of crystals of the dithionite-reduced protein in an anaerobic environment prior to being frozen in liquid nitrogen. Optical absorption spectra of crystals so obtained are shown in Figure 1 (A, B, and C paths), and

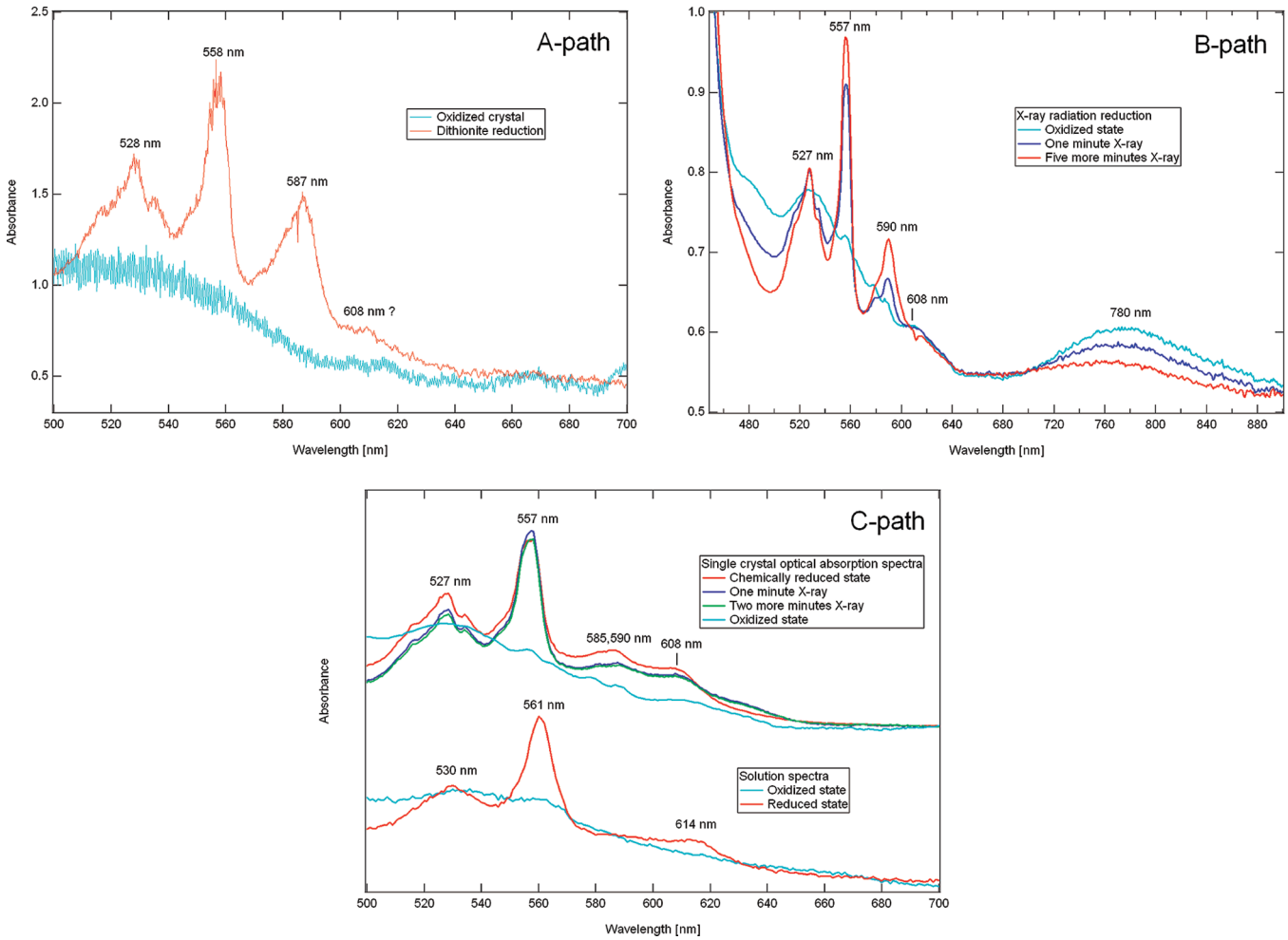

FIGURE 1: (A path) Optical absorption spectra recorded from two different crystals of cytochrome ba_3 from *T. thermophilus*. Spectrum of a crystal grown from oxidized (which is the same as the as-isolated enzyme) cytochrome ba_3, cryoprotected in the absence of dithionite and cooled to 100 K in a cryostream (cyan trace). Spectrum of a crystal grown from oxidized, as-isolated cytochrome ba_3, cryoprotected in the presence of ~10 mM dithionite and cooled to 100 K in a cryostream (red trace). Spectra were recorded at The Scripps Research Institute using the Ocean Optics USB4000 spectrophotometer. (B path) Effects of 1 Å X-ray radiation on the absorption spectra of an oxidized crystal of cytochrome ba_3 from *T. thermophilus* at 100 K. The cyan trace shows the optical absorption spectrum of this crystal prior to exposure to X-rays. The blue trace shows the optical absorption spectrum of the same crystal after exposure to an X-ray beam for 1 min. The red trace, recorded after irradiation for an additional 5 min, indicates maximum radiation-induced reduction. Spectra were recorded using the Ocean Optics QE65000 spectrometer mounted on beamline 7-1 of SSRL. (C path) Effect of X-ray radiation on the 100 K optical absorption spectrum of a single crystal of reduced cytochrome ba_3 from *T. thermophilus* (top set). The cyan trace is that of the oxidized crystal shown for the B path (top). The red trace was recorded from a different crystal grown from reduced protein (C path; see the text). The nearly overlapping blue and green traces were obtained after additional exposure to radiation. The lower set of spectra are optical absorption spectra of the oxidized (cyan) and dithionite-reduced (red) protein recorded from detergent-solubilized cytochrome ba_3. Spectra were recorded as described for the A path using the Ocean Optics USB4000 spectrometer. Spectral figures were created with IgorPro.

spectra of a solution of ba_3 are shown in the lower portion of Figure 1C; more extensive solution spectra are presented in refs *3* and *25*.

Optical Absorption Spectra of Single Crystals. Crystals formed from the as-isolated enzyme and maintained at 100 K in a cryostream exhibit a broad, generally featureless optical absorption spectrum [cyan traces in Figure 1 (A, B, and C paths)] comparable to spectra recorded in solution at room temperature (cyan trace, lower set, Figure 1, C path). The broad absorption band at ~780 nm, cyan trace for the B path in Figure 1, probably arises from the oxidized form of the weakly absorbing Cu_A center, although this feature is not observed in all crystals of the as-isolated enzyme that we have examined.

A Path. When a crystal of oxidized enzyme at room temperature is exposed to a cryoprotectant solution containing ~10 mM dithionite for ~10 s prior to being frozen in liquid nitrogen, its optical spectrum shows distinct features that are reasonably assigned to the 6cLS ferrous heme *b*, ~528 and ~558 nm (Figure 1 A path). In addition, an intense but unexpected absorption envelope appears near ~587 nm.

B Path. As shown by the blue and red traces for the B path in Figure 1, a crystal of the as-isolated, oxidized enzyme, maintained in a cryostream at ~100 K, becomes reduced upon exposure to the X-ray beam. Exposure for as little as 1 min (see Experimental Procedures) caused the appearance of the sharp absorption bands (~527 and ~557 nm) due to the 6cLS ferrous heme *b*, and exposure to the beam for an additional 5 min caused only a modest (≈20%) further increase in these absorption bands. Here again, the unexpected ~590 nm band is also seen, but probably because the bands appear sharper in this configuration (see Experimental Procedures), it has a shoulder at ~585 nm.

C Path. Spectra of crystals obtained from the dithionite-

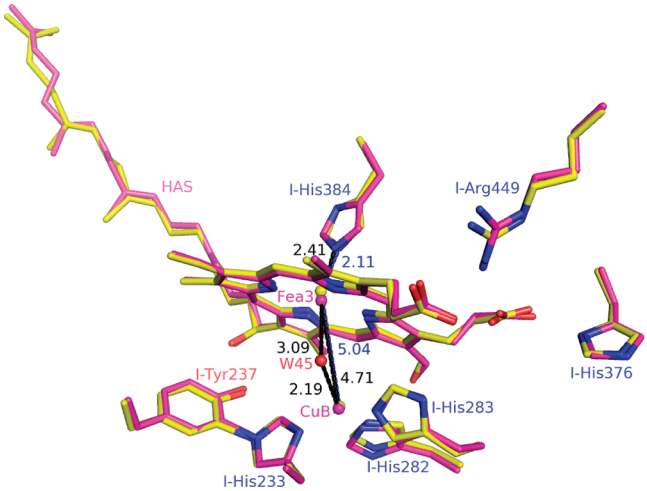

FIGURE 2: Superimposition of binuclear site structures of *T. thermophilus* cytochrome ba_3 in oxidized, as-isolated crystals (magenta, reduced by the B path) and in crystals grown from chemically reduced protein (C path, yellow). The two structures were superimposed using COOT and then displayed with PyMOL. Additional metric data are given in Table SI_1 of the Supporting Information.

reduced enzyme, cryocooled in liquid nitrogen and examined at 100 K, also exhibited strong absorption bands due to reduced heme *b* (~527 and ~557 nm), relatively weak absorption near ~585 and 590 nm, and yet a new and stronger band near ~608 nm (Figure 1, C path).

We were concerned that additional exposure to X-ray radiation would cause further changes in the optical spectrum. However, beyond the possible emergence of a broadband at ~630 nm, this did not occur, indicating that one-electron reduction is not followed by, for example, further reduction of the porphyrin π-system (Figure 1, C path). With this concern allayed, we determined the structures of the two, chemically reduced forms of cytochrome ba_3, i.e., those obtained by A- and C paths, and compared them to the structure resulting from the B path.

X-ray Crystallographic Structures. The root-mean-square (rms) differences among the structure of ba_3 in chemically reduced crystals (A path), crystals of the as-isolated protein (B path), and crystallized reduced protein (C path) are on the order of ~0.3 Å. A few residues located on the surface of the protein show slightly larger deviations, because they reside in flexible loops. No significant change was observed at the Cu_A, Cu_B, or heme *b* metal. However, small changes do occur in and around the dinuclear site (Figure 2). These include movement of the Fe_{a3} atom as well as possible changes in the interaction between the guanidinium group of I-Arg449 and the D-ring propionate of heme a_3, while the interaction between the A-ring propionate O1D and ND1 of I-His376 is unchanged. Further work is required to determine if these small changes are important to the enzyme's mechanism.

To avoid bias in restrained refinement and more accurately determine the distance between iron and copper atoms, anomalous difference maps were created (Figure 3a−c). At high contour levels (4σ), these illustrate the shift in metal positions. The Fe_{a3}−Cu_B distances were derived by refining coordinates of the two atoms against the anomalous scattering data (see Experimental Procedures). Metric comparisons of the dinuclear center in the chemically reduced structure with that in the as-isolated cytochrome ba_3 structure are presented in Table SI_1 of the Supporting Information. The distance between Fe_{a3} and Cu_B, which is 4.7 Å in crystals of the as-isolated protein (B path), increases to 5.1 and 5.0 Å in reduced crystals (A path) and in crystals grown from the chemically reduced protein (C path), respectively. The shorter 4.7 Å distance of the B path structure is comparable to the 4.4 Å distance obtained previously from higher-resolution structures that were studied under different conditions (Table SI_1 of the Supporting Information, and Protein Data Bank entries 1XME and 1EHK).

In the structures reported here, the greater Fe_{a3}−Cu_B separation results mainly from movement of the Fe_{a3} atom out of the plane of the porphyrin toward the NE2 atom of I-His384, while the Cu_B atom remains in its original position (Figure 2). This movement of the Fe_{a3} atom is accommodated and perhaps even caused by shortening of the I-His384 NE2−Fe_{a3} interaction by ~0.3 Å in the A and C path structures, suggesting that I-His384 and Cu_B are anchored in protein space while the Fe_{a3} atom can move along the normal to the heme plane. Such differences may find their origin in the chemistry that is occurring in the reaction chamber (see, for example, ref *7*). Note that in the structure of cytochrome aa_3 of *Rhodobacter sphaeroides* reported by Qin et al. (*26*) there appear to be two O atoms in the as-isolated enzyme.

The other significant finding is that the water molecule residing between Cu_B and Fe_{a3} in the B path structure (Figure 3B and Protein Data Bank entries 1EHK and 1XME) is no longer present in either structure of chemically reduced ba_3 (A and C paths, Figure 3A,C). A $2F_o - F_c$ map (at 1σ, not shown) indicates no connection between the two metals. Figure 3B shows the $|F_o| - |F_c|$ map (at 4σ) indicating the presence of a strong water peak in the dinuclear center of the X-ray radiation-reduced structure (i.e., B path). The $|F_o| - |F_c|$ maps for the A and C path structures also show no significant features between the Fe_{a3} and Cu_B sites. These data indicate that an O atom resides between Cu_B and Fe_{a3} in the oxidized, as-isolated structure, but they do not reveal the metal to which this atom is coordinately bonded prior to radiation reduction (see Discussion).

DISCUSSION

Recent studies with other heme proteins (see refs *27*−*29* and references cited therein) have provided evidence for spectral and/or structural changes induced by intense X-ray radiation. The chemical, spectral, and structural results described here for *Thermus* cytochrome ba_3 can be understood in terms of the following. First, crystalline, oxidized cytochrome ba_3 can be fully reduced by a short incubation in a buffered cryosolution containing ~10 mM $Na_2S_2O_4$, or alternatively, crystals can be formed from the reduced protein in dithionite-containing mother liquor and maintained O_2-free. Second, because electrons formed during X-ray photolysis of water (*27*) are strongly reducing, it might have been expected that synchrotron-derived X-ray beams, with their high photon flux, would result in reduction of the metal centers of cytochrome *c* oxidases (*30*−*32*). However, as shown in the C path of Figure 1, the X-ray beam does not significantly alter the heme chromophores beyond the level

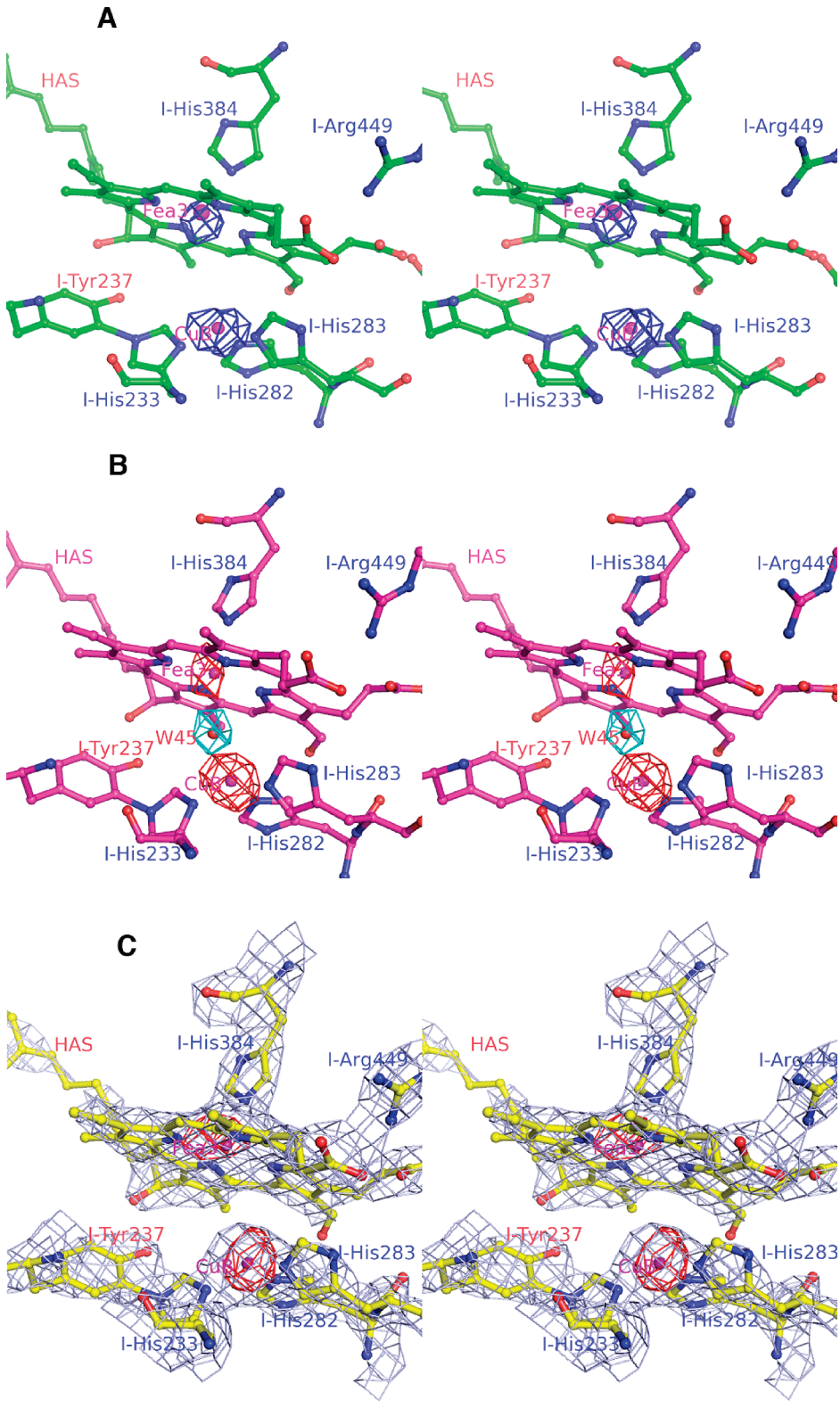

FIGURE 3: Stereoviews (cross-eyed) of the binuclear sites of three *T. thermophilus* cytochrome ba_3 oxidase structures: (A) crystallized, chemically reduced form (see Figure 1 A path for spectra); (B) crystallized, X-ray radiation-reduced form corresponding to previously reported structures considered at the time to be "oxidized" (see Figure 1 B path for spectra) [one water molecule at the binuclear site (cyan $F_o - F_c$ "omit" map contoured at 4σ) is present in B path crystals]; and (C) chemically reduced, crystallized form (see Figure 1 C path for spectra). The $2F_o - F_c$ map illustrates the clean absence of electron density (2σ) between Fe_{a3} and Cu_B in the C path structure. The anomalous difference maps are contoured at 4σ for Cu_B and Fe_{a3}.

of reduction already effected by dithionite. Third, atom motions that might normally accompany reduction of the enzyme are likely to be resisted by the protein itself and possibly (?) crystal lattice forces, both of which will be less inclined to undergo change at 100 K. This is particularly important following the B path. If the radiation-induced reduction of metal centers leads to unstable reduced states, e.g., those having a high affinity for protons (see ref *7* for

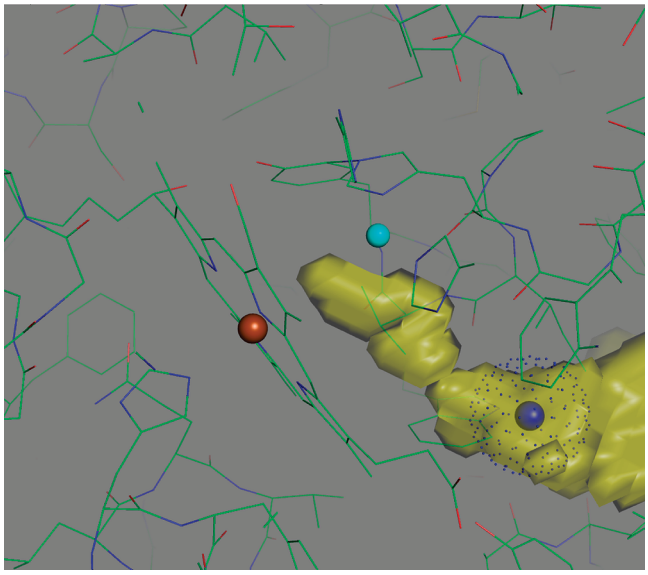

FIGURE 4: Extension of the O_2 channel (yellow; see ref *8*) in chemically reduced *Thermus* ba_3 oxidase, as determined using VOIDOO (see Experimental Procedures). Colored spheres mark the positions of Cu_B (cyan), Fe_{a3} (brown), and Xe1 (blue). Dots associated with the latter indicate the van der Waals radius of Xe. This figure was created using PyMOL.

a review), then movement of these within the protein may create forces that are resisted under these conditions, thereby resulting in nonequilibrium structures. In contrast, when crystals are exposed to dithionite at room temperature, the metal centers may relax to the states observed along the A or C path. Applying these facts and concepts allows a tentative interpretation of both spectral and structural data.

Spectral Changes. Upon chemical reduction of the enzyme in solution, all sites will be reduced [Cu_A, heme *b*, and the Cu_B-Fe_{a3} dinuclear center (*3, 16, 25, 33*)], and each heme will exhibit a unique absorption spectrum. Heme *b* is a typical 6cLS electron carrier, known to be in rapid redox equilibrium with Cu_A (*25*). Its unique optical spectrum serves as a sensitive indicator of enzyme reduction, and its features are similar in crystals obtained along each path as well as in solution (Figure 1, C path).

By contrast, heme a_3 contributes unique, path-dependent spectra in the form of the ~585 and 590 nm envelope in all crystalline forms, and the ~608 nm peak observed in C path crystals. Absorption of light at ~590 nm is commonly observed with the 6cLS forms of ferrous heme a_3 such as its CO (*34*) and CN^- complexes (*35*). However, all the structures reported here clearly demonstrate the absence of a sixth ligand to Fe_{a3}. Hence, the ~590 nm envelope cannot be due to a 6cLS ferrous heme a_3. Although the reason for a spin change is not known, we tentatively propose that a 5cLS electronic configuration of ferrous heme a_3 is responsible for the ~585 and 590 nm envelope in all the crystal forms. Such an unusual electronic configuration could result from structural trapping at 100 K. It is important to note that these optical transitions have been observed only at low temperatures in the crystalline state.

Crystals from the C path, however, exhibit rather little ~585 and 590 nm absorption compared to A and B path crystals but instead have a significant band at ~608 nm. We suggest this represents the 5cHS electronic configuration of ferrous heme a_3 and would correspond to the low-temperature, crystal-shifted version of the solution absorption band (Figure 1, C path).

Structural Changes. Each path for obtaining reduced, crystalline ba_3 leads to overall similar structures. However, each form is spectrally distinct, and therefore, at some level, it must also be structurally different. Heme a_3 and Cu_B, forming the O_2 reduction/H^+ pumping site, must pass through numerous electronation and protonation states during catalysis (*7, 36, 37*). Small structural changes will be outside the current resolution, but they are likely to be important in enzyme function. Two real differences between chemical and radiation reduction are movement of Fe_{a3} away from Cu_B by ~0.3 Å and loss of the inter-metal O atom. These changes are likely to be mechanistically important because they prepare the reaction chamber to bind an O_2 molecule. Reduction of the metals leads to an increase in the volume of the reaction chamber and causes the appearance of apposing, open-coordination positions on those metals, which appear perfectly evolved to bind O_2 and reduce it to a bridging peroxo dianion (see ref 100 of ref *7*). As summarized in Table SI_1 of the Supporting Information, a similar Cu_B-Fe_{a3} distance change also occurs in A1-type oxidases.

As might be expected, the O_2 channel (*8*) should extend to include the space between Fe_{a3} and Cu_B, which is the ultimate binding site for dioxygen. Figure 4 shows the VOIDOO representation of this extended channel with a blue sphere to mark the penultimate O_2-binding site (the Xe1 position described in ref *8*).

Finally, the nature of the inter-metal O atom in the oxidized protein is potentially of great mechanistic importance because its position and protonation state (O^{2-}, HO^-, or $H_2O°$) will affect the overall charge and the distribution of charge throughout the active site (*7*).

ACKNOWLEDGMENT

We thank Dr. Elizabeth Getzoff for the use of her microscope objectives, crystal mounting equipment, and cryo control system and Dr. David Goodin for the use of his Ocean Optics USB4000 spectrophotometer.

SUPPORTING INFORMATION AVAILABLE

One table listing the $Fe_{a3}-Cu_B$ distances in several cytochrome *c* oxidase structures. This material is available free of charge via the Internet at http://pubs.acs.org.

REFERENCES

1. Richter, O.-M. H., and Ludwig, B. (2003) Cytochrome *c* oxidase: Structure, function, and physiology of a redox driven molecular machine. *Rev. Physiol. Biochem. Pharmacol. 147*, 47–74.
2. Brunori, M., Giuffre, A., and Sarti, P. (2005) Cytochrome *c* oxidase, ligands and electrons. *J. Bioinorg. Chem. 99*, 324–326.
3. Zimmermann, B. H., Nitsche, C. I., Fee, J. A., Rusnak, F., and Munck, E. (1988) Properties of a copper-containing cytochrome ba_3: A second terminal oxidase from the extreme thermophile *Thermus thermophilus*. *Proc. Natl. Acad. Sci. U.S.A. 85*, 5779–5783.
4. Oertling, W. A., Surerus, K. K., Einarsdottir, O., Fee, J. A., Dyer, R. B., and Woodruff, W. H. (1994) Spectroscopic characterization of cytochrome ba_3, a terminal oxidase from *Thermus thermophilus*: Comparison of the a_3/Cu_B site to that of bovine cytochrome aa_3. *Biochemistry 33*, 3128–3141.

5. Soulimane, T., Buse, G., Bourenkov, G. B., Bartunik, H. D., Huber, R., and Than, M. E. (2000) Structure and mechanism of the aberrant ba_3-cytochrome *c* oxidase from *Thermus thermophilus*. *EMBO J. 19*, 1766–1776.
6. Hunsicker-Wang, L. M., Pacoma, R. L., Chen, Y., Fee, J. A., and Stout, C. D. (2005) A novel cryoprotection scheme for enhancing the diffration of crystals of the recombinant, integral-membrane cytochrome ba_3 from *Thermus thermophilus*. *Acta Crystallogr. D61*, 340–343.
7. Fee, J. A., Case, D. A., and Noodleman, L. (2008) Toward a chemical mechanism of proton pumping by the B-type cytochrome *c* oxidases: Application of density functional theory to cytochrome *ba3* of *Thermus thermophilus*. *J. Am. Chem. Soc. 130*, 15002–15021.
8. Luna, V. M. M., Chen, Y., Fee, J. A., and Stout, C. D. (2008) Crystallographic studies of Xe and Kr binding within the large internal cavity of cytochrome *ba3* from *Thermus thermophilus*: Structural analysis and role of oxygen transport channels in the heme-Cu oxidases. *Biochemistry 47*, 4657–4665.
9. Pereira, M. M., Santana, M., and Teixeira, M. (2001) A novel scenario for the evolution of haem-copper oxygen reductases. *Biochim. Biophys. Acta 1505*, 185–208.
10. Harrenga, A., and Michel, H. (1999) The cytochrome c oxidase from *Paracoccus denitrificans* does not change the metal center ligation upon reduction. *J. Biol. Chem. 274*, 33296–33299.
11. Tsukihara, T., Shimokata, K., Katayama, Y., Shimada, H., Muramoto, K., Aoyama, H., Mochizuki, M., Shinzawa-Itoh, K., Yamashita, E., Yao, M., Ishimura, Y., and Yoshikawa, S. (2003) The low-spin heme of cytochrome *c* oxidase as the driving element of the proton-pumping process. *Proc. Natl. Acad. Sci. U.S.A. 100*, 15304–15309.
12. Yoshikawa, S., Shinzawa-Itoh, K., and Tsukihara, T. (1998) Crystal structure of bovine heart cytochrome c oxidase at 2.8 Å resolution. *J. Bioenerg. Biomembr. 30*, 7–14.
13. Tsukihara, T., Shimokata, K., Katayama, Y., Shimada, H., Muramoto, K., Aoyama, H., Mochizuki, M., Shinzawa-Itoh, K., Yamashita, E., Yao, M., Ishimura, Y., and Yoshikawa, S. (2003) The Low-Spin Heme of Cytochrome C Oxidase as the Driving Element of the Proton-Pumping Process. *Proc. Natl. Acad. Sci. U.S.A. 100*, 15304–15309.
14. Liu, B., Luna, V. M., Chen, Y., Stout, C. D., and Fee, J. A. (2007) An unexpected outcome of surface engineering an integral membrane protein: improved crystallization of cytochrome *ba3* from *Thermus thermophilus*. *Acta Crystallogr. F63*, 1029–1034.
15. Michel, B., and Bosshard, H. R. (1989) Oxidation of cytochrome c by cytochrome c oxidase: Spectroscopic binding studies and steady-state kinetics support a conformational transition mechanism. *Biochemistry 28*, 244–252.
16. Chen, Y., Hunsicker-Wang, L. M., Pacoma, R. L., Luna, E., and Fee, J. A. (2005) A homologous expression system for obtaining engineered cytochrome ba_3 from *Thermus thermophilus* HB8. *Protein Expression Purif. 40*, 299–318.
17. Hadfield, A. T., and Hajdu, J. (1993) A fast and portable microspectrophotometer for time-resolved X-ray diffraction experiments. *J. Appl. Crystallogr. 26*, 839–842.
18. Bailey, S. (1994) *Acta Crystallogr. D,* 760–763.
19. Read, R. J. (2001) Pushing the boundaries of molecular replacement with maximum likelihood. *Acta Crystallogr. D57*, 1373–1382.
20. Murshudov, G. N., Vagin, A. A., and Dodson, E. J. (1999) Refinement of macromolecular structures by the maximum-likelihood method. *Acta Crystallogr D53*, 240–255.
21. Brunger, A. T. (1992) *X-PLOR*, version 3.0, Yale University Press, New Haven, CT.
22. Emsley, P., and Cowtan, K. (2004) Coot: Model-building tools for molecular graphics. *Acta Crystallogr. D60*, 2126–2132.
23. Kleywegt, G. J., and Jones, T. A. (1994) Detection, delineation, measurement, and display of cavities in macromolecular structures. *Acta Crystallogr. D50*, 178–185.
24. DeLano, W. L. (2002) *The PyMOL Molecular Graphics System*, DeLano Scientific, San Carlos, CA.
25. Farver, O., Chen, Y., Fee, J. A., and Pecht, I. (2006) Electron transfer among the CuA-, heme b- and heme a3-centers of *Thermus thermophilus* cytochrome ba_3. *FEBS Lett. 580*, 3417–3421.
26. Qin, L., Hiser, C., Mulichak, A., Garavito, R. M., and Ferguson-Miller, S. (2006) Identification of conserved lipid/detergent-binding sites in a high-resolution structure of the membrane protein cytochrome *c* oxidase. *Proc. Natl. Acad. Sci. U.S.A. 103*, 16117–16122.
27. Garman, E. F., and Owen, R. L. (2006) Cryocooling and radiation damage in macromolecular crystalography. *Acta Crystallogr. D62*, 32–247.
28. Unno, M., Chen, H., Kusama, S., Shaik, S., and Ikeda-Saito, M. (2007) Structural characterization of the fleeting ferric peroxo species in myoglobin. Experiment and theory. *J. Am. Chem. Soc. 129*, 13394–13395.
29. Denisov, I. G., Victoria, D. C., and Sligar, S. G. (2007) Cryoradiolytic reduction of heme proteins: Maximizing dose-dependent yield. *Radiat. Phys. Chem. 76*, 714–721.
30. Tsukihara, T., Aoyama, H., Yamashita, E., Tomizaki, T., Yamaguchi, H., Shinzawa-Itoh, K., Nakashima, R., Yaono, R., and Yoshikawa, S. (1996) The whole structure of the 13-subunit oxidized cytochrome c oxidase at 2.8 Å. *Science 272*, 1136–1144.
31. Iwata, S., Ostermeier, C., Ludwig, B., and Michel, H. (1995) Structure at 2.8 Å resolution of cytochrome c oxidase from *Paracoccus denitrificans*. *Nature 376*, 660–669.
32. Svensson-Ek, M., Abramson, J., Larsson, G., Törnath, S., Brzezinski, P., and Iwata, S. (2002) The X-ray crystal structures of wild-type and EQ(I-286) mutant cytochrome *c* oxidases from *Rhodobacter sphaeroides*. *J. Mol. Biol. 321*, 329–339.
33. Sousa, F. L., Verissimo, A. F., Baptista, A. M., Soulimane, T., Teixeira, M., and Pereira, M. M. (2008) Redox properties of *Thermus thermophilus* ba_3: Different electron-proton coupling in oxygen reductases? *Biophys. J. 94*, 2434–2441.
34. Goldbeck, R. A., Einarsdottir, O., Dawes, T. D., O'Connor, D. B., Surerus, K. K., Fee, J. A., and Kliger, D. S. (1992) Magnetic circular dichroism study of cytochrome ba_3 from *Thermus thermophilus*: spectral contributions from cytochromes *b* and a_3 and nanosecond spectroscopy of CO photodissociation intermediates. *Biochemistry 31*, 9376–9387.
35. Surerus, K. K., Oertling, W. A., Fan, C., Gurbiel, R. J., Einarsdottir, O., Antholine, W. E., Dyer, R. B., Hoffman, B. M., Woodruff, W. H., and Fee, J. A. (1992) Reaction of cyanide with cytochrome ba_3 from *Thermus thermophilus*: Spectroscopic characterization of the $Fe(II)a_3$-CN·$Cu(II)_B$-CN complex suggests four ^{14}N atoms are coordinated to CuB. *Proc. Natl. Acad. Sci. U.S.A. 89*, 3195–3199.
36. Siletsky, S., Soulimane, T., Azarkina, N., Vygodina, T. V., Buse, G., Kaulen, A., and Konstantinov, A. (1999) Time-resolved generation of a membrane potential by ba_3 cytochrome oxidase from *Thermus thermophilus*. *FEBS Lett. 457*, 98–102.
37. Smirnova, I. A., Zaslavsky, D., Fee, J. A., Gennis, R. B., and Brzezinski, P. (2008) Electron and proton transfer in the ba_3 oxidase from *Thermus thermophilus*. *J. Bioenerg. Biomembr. 40*, 281–287.

BI801759A